Kumar, Pramod; Peotta, Sebastiano; Takasu, Yosuke; Takahashi, Yoshiro; Törmä, Päivi

Flat band induced non-Fermi liquid behavior of multicomponent fermions

Published in:
Physical Review A

DOI:
10.1103/PhysRevA.103.L031301

Published: 03/03/2021

Document Version
Publisher's PDF, also known as Version of record

Letter

Flat-band-induced non-Fermi-liquid behavior of multicomponent fermions

Pramod Kumar,[1] Sebastiano Peotta,[1,2,3] Yosuke Takasu,[4] Yoshiro Takahashi,[4] and Päivi Törmä[1]

[1]*Department of Applied Physics, Aalto University, FI-00076 Aalto, Finland*

[2]*Computational Physics Laboratory, Physics Unit, Faculty of Engineering and Natural Sciences, Tampere University, P.O. Box 692, FI-33014 Tampere, Finland*

[3]*Helsinki Institute of Physics, P.O. Box 64, FI-00014 Helsinki, Finland*

[4]*Department of Physics, Graduate School of Science, Kyoto University, Kyoto 606-8502, Japan*

(Received 13 May 2020; revised 1 February 2021; accepted 15 February 2021; published 3 March 2021)

We investigate multicomponent fermions in a flat band and predict experimental signatures of non-Fermi-liquid behavior. We use dynamical mean-field theory to obtain the density, double occupancy and entropy in a Lieb lattice for $\mathcal{N} = 2$ and $\mathcal{N} = 4$ components. We derive a mean-field scaling relation between the results for different values of $\mathcal{N}$, and study its breakdown due to beyond mean-field effects. The predicted signatures occur at temperatures above the Néel temperature and persists even in the presence of a trapping potential, thus they are observable in current ultracold gas experiments.

DOI: 10.1103/PhysRevA.103.L031301

As interaction effects are enhanced in a flat Bloch band, remarkable ordered phases such as flat band ferromagnetism [1] and superconductivity [2–5] have been predicted. Quasi-flat bands, whose bandwidth is comparable or smaller than the typical energy scale of interactions, seem to explain why the critical temperature of the superconducting state recently observed in magic-angle twisted bilayer graphene is large compared to the Fermi energy [6–9]. Also the normal states above the critical temperature of ordered phases are expected to be nontrivial: since a noninteracting flat band system does not have a Fermi surface and is an insulator at any filling, a Landau-Fermi liquid is generally not expected [10,11].

The strange metal phase of copper-based superconductors (cuprates) is the most well known example of a non-Fermi-liquid phase, and is still not fully understood [12–14]. The repulsive Fermi-Hubbard model on a square lattice is considered a minimal model for the cuprates, and according to recent numerical studies the crossover from a metallic (Fermi liquid) state at weak coupling to an antiferromagnetic insulator at strong coupling occurs through an intermediate non-Fermi liquid [15]. Strange metal behavior has been observed experimentally both on the square lattice Hubbard model realized with optical lattices [16] and in twisted bilayer graphene [17].

For the Hubbard model on lattice geometries other than the simple square lattice, the existence of a non-Fermi-liquid normal state is currently much less investigated. In the case of the Lieb lattice—a typical flat band model—clear signatures of non-Fermi-liquid behavior have been found at low temperature in the self-energy and quasiparticle weight behavior by means of dynamical mean-field theory [18,19]. Experimental evidence of non-Fermi-liquid behavior on composite lattice geometries such as the Lieb lattice is at present lacking. Here, we identify and calculate the experimental signatures of a non-Fermi liquid that can be most directly probed in ultracold gas experiments on composite lattice geometries.

Since spin-related order or correlations, for instance magnetic order and pairing, are typically induced by a flat band, it is of interest to ask what happens if one goes beyond the case of spin-1/2 fermions [20–24]. Recently a degenerate gas of bosonic isotopes of ytterbium was loaded in a Lieb lattice [25], and the same can be done with fermionic ones [26]. This would provide the quantum simulation of the Fermi-Hubbard model with $\mathcal{N} > 2$ spin components [21,27,28], in a paradigm flat band system. We investigate the non-Fermi-liquid normal state of the repulsive Hubbard model on a Lieb lattice for both $\mathcal{N} = 2$ and $\mathcal{N} = 4$ cases, and find a scaling relation between them. We predict that the non-Fermi-liquid properties manifest in the sublattice-resolved double occupancy and entropy—all quantities that can be observed in ultracold gas experiments [29–32]—in contrast to predictions regarding the self-energy [18] that are difficult to probe. In particular, the sublattice-resolved double occupancy for ytterbium atoms can be measured by combining the sublattice-mapping technique, already demonstrated for the Lieb lattice [25,33], with photoassociation-induced atom loss [34].

As the temperatures considered here are above the magnetically ordered phase, as compared to the previous works [18,19] where low temperature magnetically ordered phases were explored, standard ultracold gas setups can be used to verify our predictions and to experimentally demonstrate the non-Fermi-liquid nature of a flat band system for the first time. Flat band lattices have been demonstrated with ultracold gas setups [25,35], and the Lieb lattice has been recently realized also in atomic scale artificial matter [36–38] and photonic systems [39–43]. Our calculations in the $\mathcal{N} = 2$ case are relevant for non-Fermi-liquid physics in a variety of systems, while ultracold ytterbium and strontium gases in the electronic ground state $^1S_0$ [44–48] provide both the $\mathcal{N} = 2$ and $\mathcal{N} = 4$ cases and allow testing of the predicted scaling relation.

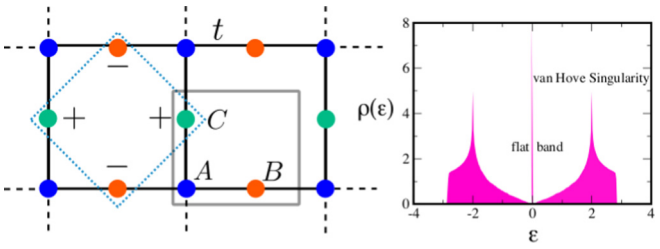

FIG. 1. (a) 2D Lieb lattice: The convention for the unit cell (grey square box) and the labeling of the three sublattices ($\alpha = A, B, C$) are shown. The links represent hoppings with magnitude t. A localized state of the flat band is the linear superposition of the four sites of the B and C sublattices inside the dashed square box. (b) The density of states $\rho(\varepsilon)$ of the noninteracting model.

Model and methods. We consider in this work a Fermi-Hubbard model defined on the two-dimensional Lieb lattice, which features a flat band at zero energy [5]. The tight-binding model with nearest-neighbor hoppings on the Lieb lattice and its density of states are shown in Fig. 1. The fermionic annihilation (creation) operator relative to sublattice α and unit cell $\mathbf{i} = (i_1, i_2)^T$ is $\hat{c}_{\mathbf{i}\alpha\sigma}$ ($\hat{c}^\dagger_{\mathbf{i}\alpha\sigma}$), while the occupation number operator is $\hat{n}_{\mathbf{i}\alpha\sigma} = \hat{c}^\dagger_{\mathbf{i}\alpha\sigma}\hat{c}_{\mathbf{i}\alpha\sigma}$. The component (or "spin") index σ labeling the fermionic operators takes values $\sigma = 1, \ldots, \mathcal{N}$, and we consider the case of four-component fermions (spin-3/2, $\mathcal{N} = 4$) on top of the usual two (spin-1/2, $\mathcal{N} = 2$). With this notation, the noninteracting Hamiltonian $\hat{\mathcal{H}}_0 = \sum_{\mathbf{i},\mathbf{j},\alpha,\beta,\sigma} K_{\alpha,\beta}(\mathbf{i}-\mathbf{j})\hat{c}^\dagger_{\mathbf{i}\alpha\sigma}\hat{c}_{\mathbf{j}\beta\sigma} - \mu\sum_{\mathbf{i},\alpha,\sigma}\hat{n}_{\mathbf{i}\alpha\sigma}$, where $K_{\alpha,\beta}(\mathbf{i}-\mathbf{j})$ encodes the hopping matrix elements of magnitude t between the nearest-neighbor sites in the Lieb lattice (see Fig. 1 and Ref. [49]). The hopping matrix is independent of the spin index σ, thus $\hat{\mathcal{H}}_0$ possesses an internal SU($\mathcal{N}$) spin symmetry. In the following we use t as the energy scale and set $t = \hbar = k_B = 1$.

The full many-body Hamiltonian $\hat{\mathcal{H}} = \hat{\mathcal{H}}_0 + \hat{\mathcal{H}}_{\text{int}}$ is the sum of the noninteracting Hamiltonian and an interaction term $\hat{\mathcal{H}}_{\text{int}} = U\sum_{\mathbf{i},\alpha}\hat{d}_{\mathbf{i}\alpha} - U(\mathcal{N}-1)\hat{N}/2 + \text{const.}$, which is the generalization of the usual Hubbard interaction term for $\mathcal{N} \geqslant 2$ and preserves the SU($\mathcal{N}$) symmetry as well.

The operator $\hat{d}_{\mathbf{i}\alpha} = \sum_{\sigma<\sigma'}\hat{n}_{\mathbf{i}\alpha\sigma}\hat{n}_{\mathbf{i}\alpha\sigma'}$ is the double occupancy operator for $\mathcal{N}$-component fermions and $\hat{N} = \sum_{\mathbf{i},\alpha,\sigma}\hat{n}_{\mathbf{i}\alpha\sigma}$ is the total particle number operator. We consider only the case of repulsive interactions ($U > 0$). In the following we focus on the expectation values of $d_{\mathbf{i}\alpha} = \langle\hat{d}_{\mathbf{i}\alpha}\rangle$ and $n_{\mathbf{i}\alpha} = \sum_\sigma\langle\hat{n}_{\mathbf{i}\alpha\sigma}\rangle$ as the main observables. We compute them using dynamical mean-field theory (DMFT) [50,51] with the continuous time quantum Monte Carlo as impurity solver [49].

The filling of the lattice is defined as $n = \sum_\alpha n_\alpha$, thus $n = 3\mathcal{N}/2$ corresponds to half filling for $\mathcal{N}$-component fermions. In our computations, we set the temperature high enough so that magnetic ordering does not occur and the SU($\mathcal{N}$) symmetry is unbroken. As a consequence, the expectation values are also independent of the spin index, that is $\langle\hat{n}_{\mathbf{i}\alpha\sigma}\rangle = \langle\hat{n}_{\mathbf{i}\alpha\sigma'}\rangle = n_{\mathbf{i}\alpha}/\mathcal{N}$ for all σ, σ' and $\langle\hat{n}_{\mathbf{i}\alpha\sigma_1}\hat{n}_{\mathbf{i}\alpha\sigma_2}\rangle = \langle\hat{n}_{\mathbf{i}\alpha\sigma_3}\hat{n}_{\mathbf{i}\alpha\sigma_4}\rangle = d_{\mathbf{i}\alpha}/\binom{\mathcal{N}}{2}$ for all $\sigma_1 \neq \sigma_2$, $\sigma_3 \neq \sigma_4$. Another observable of interest is the entropy per lattice site, s, which has been measured in many optical lattice experiments [32,52]. The entropy is obtained from the occupation number using the relation $s(\mu, U, T) = \frac{1}{3}\int_{-\infty}^{\mu}\partial_T n(\mu, U, T)d\mu$ [49].

Entropy and double occupancy. If $f(T, n, U)$ denotes the free energy per lattice site, one has $s = -\partial_T f$ while the derivative with respect to the coupling constant U gives the double occupancy averaged over the unit cell $d = \frac{1}{3}\sum_\alpha d_\alpha = \partial_U f$. Thus one has the Maxwell's relation

$$\frac{\partial s}{\partial U} = -\frac{\partial d}{\partial T}\,. \tag{1}$$

Note that there is no sensible way to separate the entropy into contributions associated to single sublattices, which makes sense for the double occupancy. For a Fermi liquid the double occupancy decreases as temperature is increased starting from $T = 0$, attains a minimum at $T = T_F^*$, where T_F^* is the quasiparticle coherence scale, and then increases for larger temperatures [29,53]. Maxwell's relation (1) provides an explanation of this peculiar nonmonotonic behavior of the double occupancy. The entropy in a Fermi liquid is linearly proportional both to the temperature and to the quasiparticle effective mass, $s \propto m_{\text{eff}}T$, and since the effective mass generally increases with the coupling constant $\partial_U m_{\text{eff}} > 0$ for repulsive interactions [54], one has from Eq. (1) that $\partial_T d < 0$ for $T < T_F^*$. This effect is observed for instance in liquid helium-3 where it is at the root of Pomeranchuk cooling [22,23,53,55]. Pomeranchuk cooling has been demonstrated for $\mathcal{N} = 6$ component fermions loaded in a cubic lattice [28,56].

$\mathcal{N} = 2$ *components.* As shown in Fig. 2(a), in the Lieb lattice the behavior of the entropy as a function of the coupling constant U changes qualitatively depending on the filling. The triple peak structure of the entropy in Fig. 2(a) is a consequence of the density of states of the Lieb lattice, Fig. 1. The interesting observation is that for fillings close to $n = 2$ one has $\partial_U s > 0$, on the other hand for $n = 3$ the entropy decreases with U. The opposite behavior of the entropy at the two fillings $n = 2$ and $n = 3$ is emphasised in the inset Fig. 2(a). For higher temperatures [Fig. 2(b)] the entropy is always a decreasing function of U at any filling. In Fig. 2(c) we show the region in the n-U plane where the non-Fermi-liquid behavior is observed at the fixed temperature $T = 0.17$. This is the region between the grey lines where we find $\partial_U s < 0$.

The behavior of the double occupancy is consistent with that of the entropy as dictated by Maxwell's relation (1). As shown in the insets of Figs. 2(d) and 2(e) the average double occupancy is a monotonically increasing function of temperature for a half filled flat band ($n = 3$), while it is decreasing at filling $n = 2$. Moreover, the behavior of the sublattice-resolved double occupancy d_α depends qualitatively on the sublattice. We see from Figs. 2(d) and 2(e) that on sublattice A the double occupancy decreases with temperature ($\partial_T d_A < 0$), while on sublattices B and C the behavior is opposite ($\partial_T d_{B/C} > 0$). This striking difference is observed in the whole temperature range $0.15 < T < 1$ considered in Fig. 2 and is particularly evident at half filling $n = 3$. This temperature range is above the magnetic phase, which occurs at around $T \sim 0.1$ for $U = 2$ according to our DMFT simulations, and just below the quasiparticle coherence scale T_F^* at which the double occupancy on the A sublattice takes its minimum value.

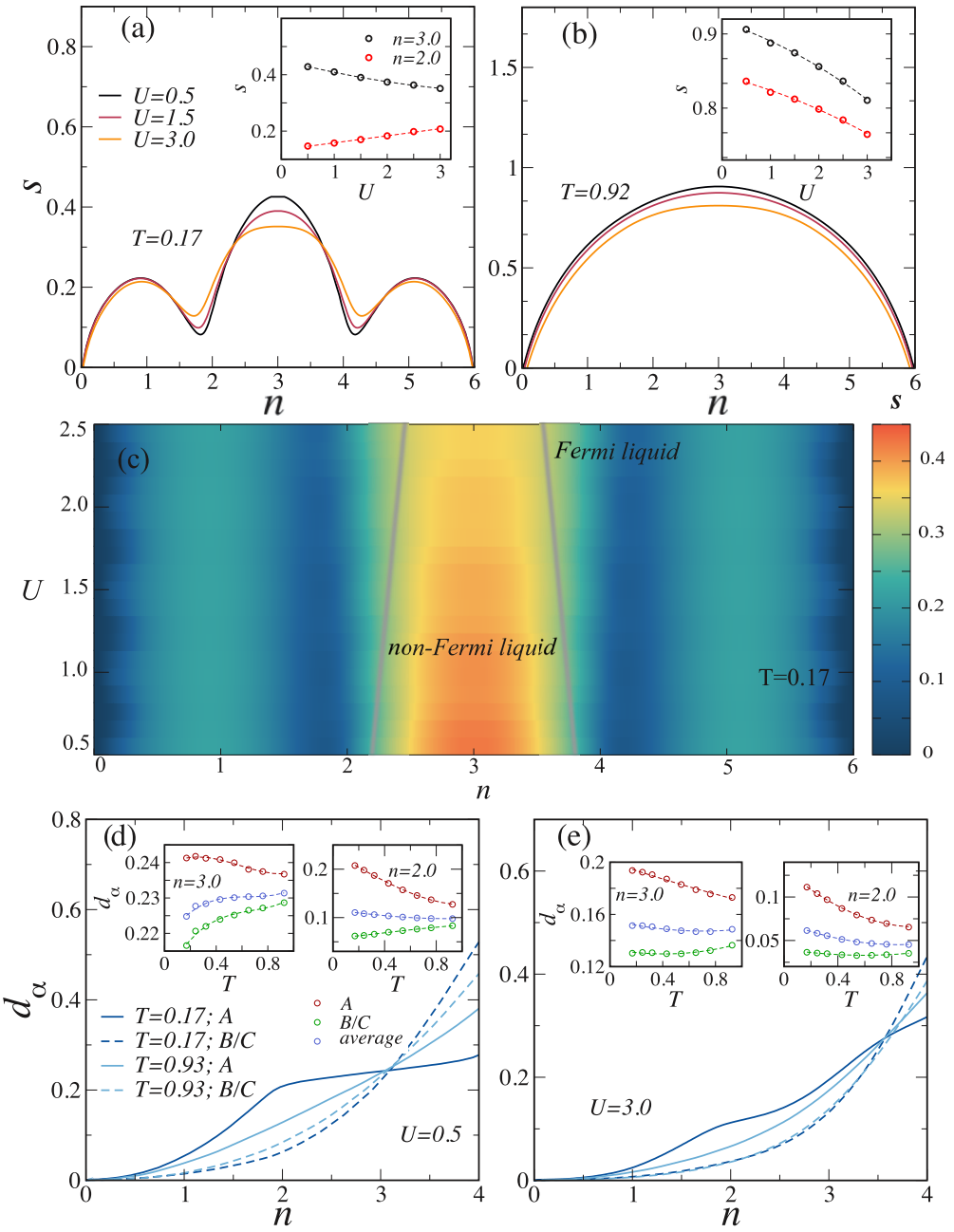

FIG. 2. (a) Entropy per lattice site s as a function of total filling $n = \sum_\alpha n_\alpha$ for $\mathcal{N} = 2$ component fermions at $T = 0.17$ and for three different values of the interaction strength. In the inset the entropy as a function of interaction strength is shown for filling $n = 3$ (half filling) and $n = 2$ (fully filled lowest band). (b) Same as panel (a), but at the different temperature $T = 0.92$. (c) Color map of the entropy in the n-U plane at the fixed temperature $T = 0.17$. In the region between the grey lines, the entropy is a decreasing function of the interaction strength ($\partial_U s < 0$), a manifestation of the flat band-induced non-Fermi-liquid behavior. (d) Sublattice resolved double occupancy d_α v. filling n at $U = 0.5$ and for the same two values of temperature of panels (a) and (b). In the insets the double occupancy (both sublattice-resolved and averaged) vs temperature at fixed fillings $n = 2, 3$ is shown. (e) Same as panel (d), but for the different value of the interaction strength $U = 3$.

The interpretation of the results shown in Fig. 2 is that the flat band is responsible for the non-Fermi-liquid behavior ($\partial_U s = -\partial_T d < 0$). Indeed, the sublattice-resolved double occupancy provides the most compelling argument in this sense. The non-Fermi-liquid behavior manifests only in the double occupancy of sublattices B and C, where the flat band states have their support (see Fig. 1), while the double occupancy in the A sublattice has the same behavior as in, for instance, a cubic lattice in the same temperature range [53]. The flat band-induced non-Fermi-liquid behavior can be observed for not too large interaction strength and modestly low temperatures. As shown in Fig. 2(b) the entropy decreases with U for all fillings at high temperatures, but this is a different effect, incoherent in nature, in which the flat band plays no role, and is observed also in simple square and cubic lattices.

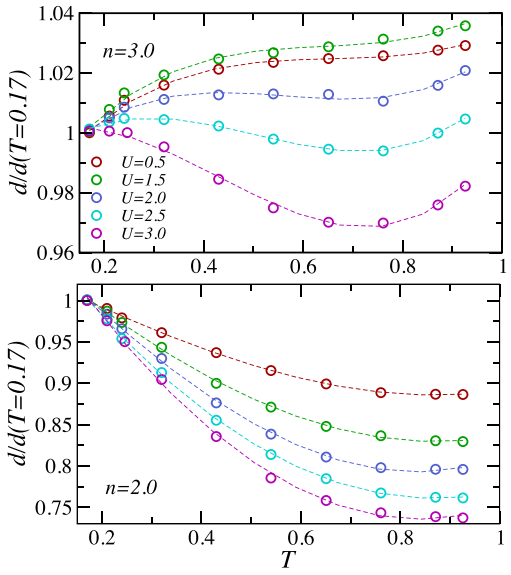

FIG. 3. Average double occupancy $d(T, n, U)$ rescaled by its value at the lowest temperature considered in this work $d(T = 0.17, n, U)$ as a function of temperature for different values of U and for fillings $n = 3$ (top panel) and $n = 2$ (bottom panel). The data for $U = 0.5$ and 3 are the same as the ones shown in the insets in Figs. 2(d) and 2(e).

Figure 3 illustrates how the flat band-induced non-Fermi-liquid behavior is eventually destroyed for large interaction strength. In Fig. 3 the average double occupancy, which does not resolve the different sublattices, is shown rescaled by its value at the lowest temperature considered here, that is $d(T, n, U)/d(T = 0.17, n, U)$, to ease the visual comparison. From the top panel of Fig. 3, one can see that the average double occupancy at $n = 3$ is a monotonically increasing function of temperature for $U = 0.5$ and 1.5. In this regime, ferromagnetic exchange $\propto U$ dominates and the interaction lifts the degeneracy due to the band flatness and lowers the entropy. A local minimum starts to develop at $U = 2$, and becomes very visible for $U = 2.5$ and 3. Indeed, as U is further increased, the antiferromagnetic exchange $\propto 1/U$ becomes important and spin entropy dominates. As consequence the Pomeranchuck effect typical of a Fermi liquid comes back. On the other hand, the standard Landau-Fermi liquid behavior always dominates in the averaged double occupancy away from half filling, as shown in the bottom panel of Fig. 3. Indeed, at filling $n = 2$ the averaged double occupancy is always a decreasing function of temperature up to $T_F^* \approx 0.9$, at which it attains its minimum as in the case of the cubic lattice [29].

$\mathcal{N} = 4$ *components.* In Fig. 4 we compare the cases of $\mathcal{N} = 2$ and $\mathcal{N} = 4$ component fermions. For $\mathcal{N} = 2$ components and $U = 2$ the behavior of the averaged double occupancy is in the crossover region in between a Landau-Fermi liquid and a non-Fermi liquid, as discussed above in relation to Fig. 3. In contrast, as shown in Fig. 4, for $\mathcal{N} = 4$ components the averaged double occupancy as a function of temperature at the same value of U looks more like that of a Landau-Fermi liquid with the characteristic minimum at $T \approx 0.9$. We

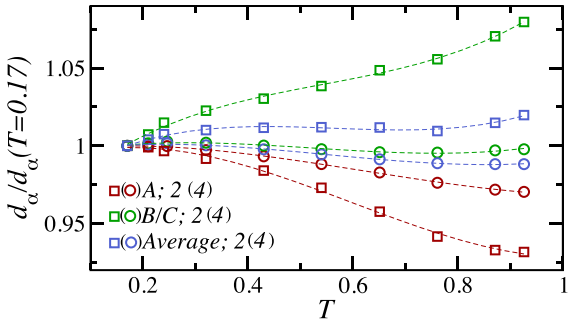

FIG. 4. Sublattice-resolved and average double occupancy at half filling and $U = 2$ rescaled by its values at the lowest temperature ($T_{\min} = 0.17$), namely $d_\alpha(T, n, U)/d_\alpha(T_{\min}, n, U)$ and $d(T, n, U)/d(T_{\min}, n, U)$, respectively.

note also that the variation of the double occupancy with temperature is reduced for $\mathcal{N} = 4$ compared to $\mathcal{N} = 2$, and that the double occupancy in the B and C sublattices does not increase monotonically as it does for $\mathcal{N} = 2$. Apparently, the flat band-induced non-Fermi-liquid behavior disappears as the number of components is increased. Here we propose a scaling argument to understand the results of Fig. 4. At the mean-field level it is possible to show [49] that the solution of the problem for a given pair of parameters $(U, \mathcal{N})$ provides also the solution for all pair of values $(U', \mathcal{N}')$ which satisfy the scaling relation

$$U(\mathcal{N} - 1) = U'(\mathcal{N}' - 1)\,. \tag{2}$$

Inserting $U' = 2, \mathcal{N}' = 4$, and $\mathcal{N} = 2$ in Eq. (2) gives $U = 6$. In other words the result for $\mathcal{N}' = 4$ components in Fig. 4 can be equivalently understood as the double occupancy of a model with $\mathcal{N} = 2$ and $U = 6$. At this large value of the coupling strength, one expects the non-Fermi-liquid behavior induced by the flat band to be suppressed, and this is indeed the case as one can see from the data for $\mathcal{N} = 4$ in Fig. 4.

In order to check the validity of the mean-field approximation underlying the scaling relation (2), we compare DMFT results for pairs of parameters $(U, \mathcal{N})$ which satisfy the scaling relation; see Fig. 5. One can observe that there is better agreement between the results for $\mathcal{N} = 2$ and $\mathcal{N}' = 4$ for the lower values of the coupling constants (left column) with respect to the higher ones (right column). Indeed, one expects the mean-field approximation to be accurate in the weakly interacting regime. Moreover a larger deviation is seen in the case of the double occupancy compared to the occupation number. This is also expected since the double occupancy is a quantity which is more sensitive to beyond mean-field correlations; indeed at the mean-field level it is simply the product of the occupation numbers ($\langle \hat{n}_{\mathbf{i}\alpha\sigma} \hat{n}_{\mathbf{i}\alpha\sigma'} \rangle = \langle \hat{n}_{\mathbf{i}\alpha\sigma} \rangle \langle \hat{n}_{\mathbf{i}\alpha\sigma'} \rangle$ for $\sigma \neq \sigma'$). From Fig. 5 one can conclude that the scaling relation holds qualitatively in the range of couplings of interest here ($0 \leqslant U \lesssim 3$ for $\mathcal{N} = 2$).

Trap effects. Combined with the lattice potential, a harmonic trap is often used in ultracold gas experiments to confine the atoms. To take into account the effect of the trapping potential, we use our DMFT results to compute the spatially averaged double occupancy, the observable defined

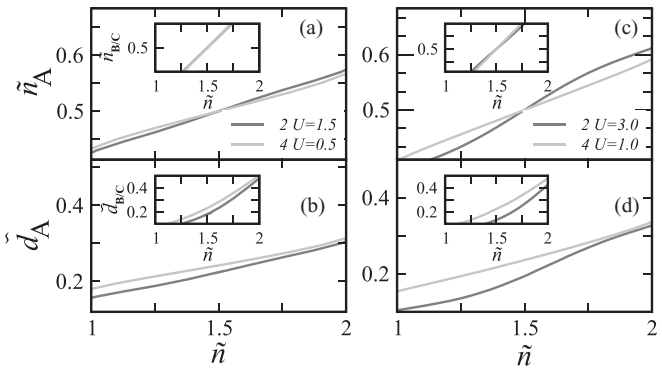

FIG. 5. Comparison of DMFT results between pairs of values $(U, \mathcal{N})$ satisfying the scaling relation (2). On the left (right) column the black lines are results for the sublattice-resolved occupation number $\tilde{n}_\alpha = n_\alpha/\mathcal{N}$ and double occupancy $\tilde{d}_\alpha = d_\alpha/\binom{\mathcal{N}}{2}$ for $U = 1.5$ $(U = 3)$ and $\mathcal{N} = 2$, while the grey lines are results for $U' = 0.5$ $(U' = 1)$ and $\mathcal{N}' = 4$. The occupation number and the double occupancy are normalized in such a way that the curves for different number of components would coincide if the mean-field approximation were exact.

by $D_\alpha = \sum_{\mathbf{i}} \langle \hat{d}_{\mathbf{i}\alpha} \rangle$ within the local density approximation [49]. As we show below, our prediction that the double occupancy in the Lieb lattice behaves in a qualitative different way depending on the sublattice [Figs. 2(d) and 2(e)] can be tested even in experimental setups that give access only to the spatially averaged double occupancy and not to the site-resolved double occupancy $d_{\mathbf{i}\alpha}$.

The quantity D_α as a function of temperature is shown in Fig. 6. The specific form of the harmonic trap potential is specified in the Supplemental Material [49]. One can see

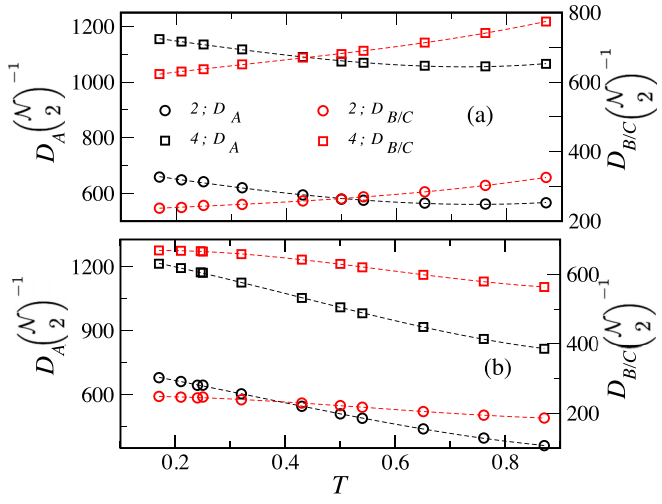

FIG. 6. (a) Sublattice-resolved and spatially averaged double occupancy $D_\alpha = \sum_{\mathbf{i}} \langle \hat{d}_{\mathbf{i}\alpha} \rangle$ vs temperature T for $U = 2$ and $\mathcal{N} = 2, 4$, in the presence of harmonic trapping. The chemical potential is fixed at $\mu = 0$ ($n = 3$ at the trap center for $\mathcal{N} = 2$, and $n = 6$ for $\mathcal{N} = 4$). (b) Same as in Fig. 4, with the only difference that the total particle number N is kept fixed, specifically $N = 1.2\times10^4 (2.4\times10^4)$ for $\mathcal{N} = 2(4)$ components.

that the different behavior of the double occupancy in the two inequivalent sublattices remains visible even in the case of the spatially averaged double occupancy. Indeed, D_A decreases with increasing temperature almost up to the highest temperatures provided in Fig. 6(a) for both $\mathcal{N} = 2$ and 4. A change in the sign of $\partial_T D_A$ is visible around $T = 0.8$. On the other hand, the spatially averaged double occupancy on the B/C sublattices is monotonically increasing with temperature for any number of components. The behavior is analogous to the thermodynamic limit shown for $\mathcal{N} = 2$ in Fig. 3. On the other hand, it might be more convenient from an experimental point of view to fix the number of particles rather than the chemical potential. The sublattice-resolved and spatially-averaged double occupancy in the case of fixed particle number is shown in Fig. 6(b). The total particle number is chosen in a such a way that the filling is approximately $n = 3$ $(n = 6)$ for $\mathcal{N} = 2$ $(\mathcal{N} = 4)$ components at the intermediate temperature $T = 0.5$. In the case of fixed particle number the local density decreases at the trap center since the atomic cloud becomes more spread out with increasing temperature. This explains why even on the B and C sublattices the double occupancy decreases with increasing temperature, if the particle number is fixed. This is simply a consequence of the fact that quite generally the double occupancy is a monotonically increasing function of the filling, as shown in Fig. 2. Even in the case of fixed particle number, the different behavior of the double occupancy on the two inequivalent sublattices is still revealed by the different rates at which D_α decreases with temperature. As shown in Fig. 6(b), the rate is higher on the A sublattice than on the B and C sublattices, which is consistent with the results for fixed chemical potential shown in Fig 6(a). This shows that our predictions can be tested even in the presence of a harmonic trap.

Conclusions. We identified signatures of non-Fermi-liquid behavior in the entropy and double occupancy in the case of the Lieb lattice with $\mathcal{N} = 2$ and $\mathcal{N} = 4$ component fermions. We showed that the nonmonotonic behavior of the double occupancy, the fingerprint of a Landau-Fermi liquid, is not present at all for sufficiently small interactions. This is a consequence of the presence of a flat band in the band structure of the Lieb lattice. Indeed, the non-Fermi-liquid behavior in the double occupancy can be observed only in the sublattices on which the flat band states have their support, the B and C sublattices, while on the A sublattice the conventional behavior is observed. We note in passing that, besides the entropy and the double occupancy, also the specific heat [57] and the spin susceptibility [58] may be used to detect the transition from a Fermi liquid to a non-Fermi liquid. Using mean-field arguments, we derived a scaling relation (2) to describe the results for different numbers of components $\mathcal{N}$. The adequacy of the mean-field approximation was investigated by means of DMFT and the scaling relation was found to be qualitatively correct in the range of couplings of interest. It is interesting to probe the validity of this scaling relation in experiments as a direct indicator of beyond mean-field effects. Our results are relevant for currently available ultracold gas setups for several reasons: temperatures above the critical one are sufficient and only sublattice-resolved, not spatially resolved, imaging of the double occupancy is required, even in the presence of a harmonic trap. Therefore,

our work opens the route for experimental investigations with ultracold gases of non-Fermi-liquid behavior induced by flat band singularities.

Acknowledgments. We thank T. I. Vanhala for useful discussions. This work was supported by the Academy of Finland under Projects No. 330384, No. 303351, No. 307419, No. 327293, and No. 318987 (QuantERA project RouTe), by the Grant-in-Aid for Scientific Research of the Ministry of Education, Culture Sports, Science, and Technology, Japan Society for the Promotion of Science (MEXT/JSPS KAKENHI, No. JP17H06138, No. JP18H05405, and No. JP18H05228), Japan Science and Technology Agency CREST (No. JPMJCR1673), and by MEXT Quantum Leap Flagship Program (MEXT Q-LEAP, No. JPMXS0118069021).

[1] A. Mielke and H. Tasaki, Ferromagnetism in the Hubbard model. Examples from models with degenerate single-electron ground states, Commun. Math. Phys. **158**, 341 (1993).

[2] N. B. Kopnin, T. T. Heikkilä, and G. E. Volovik, High-temperature surface superconductivity in topological flat-band systems, Phys. Rev. B **83**, 220503(R) (2011).

[3] T. T. Heikkilä, N. B. Kopnin, and G. E. Volovik, Flat bands in topological media, JETP Lett. **94**, 233 (2011).

[4] S. Peotta and P. Törmä, Superfluidity in topologically nontrivial flat bands, Nat. Commun. **6**, 8944 (2015).

[5] A. Julku, S. Peotta, T. I. Vanhala, D.-H. Kim, and P. Törmä, Geometric Origin of Superfluidity in the Lieb-Lattice Flat Band, Phys. Rev. Lett. **117**, 045303 (2016).

[6] L. Classen, Viewpoint: Geometry rescues superconductivity in twisted graphene, Physics **13**, 23 (2020).

[7] X. Hu, T. Hyart, D. I. Pikulin, and E. Rossi, Geometric and Conventional Contribution to the Superfluid Weight in Twisted Bilayer Graphene, Phys. Rev. Lett. **123**, 237002 (2019).

[8] A. Julku, T. J. Peltonen, L. Liang, T. T. Heikkilä, and P. Törmä, Superfluid weight and Berezinskii-Kosterlitz-Thouless transition temperature of twisted bilayer graphene, Phys. Rev. B **101**, 060505(R) (2020).

[9] F. Xie, Z. Song, B. Lian, and B. A. Bernevig, Topology-Bounded Superfluid Weight in Twisted Bilayer Graphene, Phys. Rev. Lett. **124**, 167002 (2020).

[10] M. Tovmasyan, S. Peotta, L. Liang, P. Törmä, and S. D. Huber, Preformed pairs in flat Bloch bands, Phys. Rev. B **98**, 134513 (2018).

[11] J. S. Hofmann, E. Berg, and D. Chowdhury, Superconductivity, pseudogap, and phase separation in topological flat bands, Phys. Rev. B **102**, 201112(R) (2020).

[12] C. M. Varma, P. B. Littlewood, S. Schmitt-Rink, E. Abrahams, and A. E. Ruckenstein, Phenomenology of the Normal State of Cu-O High-Temperature Superconductors, Phys. Rev. Lett. **63**, 1996 (1989).

[13] P. A. Lee, N. Nagaosa, and X.-G. Wen, Doping a Mott insulator: Physics of high-temperature superconductivity, Rev. Mod. Phys. **78**, 17 (2006).

[14] N. E. Hussey, Phenomenology of the normal state in-plane transport properties of high-T_c cuprates, J. Phys.: Condens. Matter **20**, 123201 (2008).

[15] F. Šimkovic, J. P. F. LeBlanc, A. J. Kim, Y. Deng, N. V. Prokof'ev, B. V. Svistunov, and E. Kozik, Extended Crossover from a Fermi Liquid to a Quasiantiferromagnet in the Half-Filled 2D Hubbard Model, Phys. Rev. Lett. **124**, 017003 (2020).

[16] P. T. Brown, D. Mitra, E. Guardado-Sanchez, R. Nourafkan, A. Reymbaut, C.-D. Hébert, S. Bergeron, A.-M. S. Tremblay, J. Kokalj, D. A. Huse, P. Schauß, and W. S. Bakr, Bad metallic transport in a cold atom Fermi-Hubbard system, Science **363**, 379 (2019).

[17] Y. Cao, D. Chowdhury, D. Rodan-Legrain, O. Rubies-Bigorda, K. Watanabe, T. Taniguchi, T. Senthil, and P. Jarillo-Herrero, Strange Metal in Magic-Angle Graphene with Near Planckian Dissipation, Phys. Rev. Lett. **124**, 076801 (2020).

[18] P. Kumar, T. I. Vanhala, and P. Törmä, Temperature and doping induced instabilities of the repulsive Hubbard model on the Lieb lattice, Phys. Rev. B **96**, 245127 (2017).

[19] P. Kumar, T. I. Vanhala, and P. Törmä, Magnetization, d-wave superconductivity, and non-Fermi-liquid behavior in a crossover from dispersive to flat bands, Phys. Rev. B **100**, 125141 (2019).

[20] C. Wu, J.-P. Hu, and S.-C. Zhang, Exact SO(5) Symmetry in the Spin-3/2 Fermionic System, Phys. Rev. Lett. **91**, 186402 (2003).

[21] M. A. Cazalilla and A. M. Rey, Ultracold Fermi gases with emergent $SU(\mathcal{N})$ symmetry, Rep. Prog. Phys. **77**, 124401 (2014).

[22] Z. Cai, H.-H. Hung, L. Wang, D. Zheng, and C. Wu, Pomeranchuk Cooling of SU($2n$) Ultracold Fermions in Optical Lattices, Phys. Rev. Lett. **110**, 220401 (2013).

[23] Z. Zhou, Z. Cai, C. Wu, and Y. Wang, Quantum Monte Carlo simulations of thermodynamic properties of SU($2n$) ultracold fermions in optical lattices, Phys. Rev. B **90**, 235139 (2014).

[24] Z. Zhou, D. Wang, C. Wu, and Y. Wang, Finite-temperature valence-bond-solid transitions and thermodynamic properties of interacting SU($2n$) Dirac fermions, Phys. Rev. B **95**, 085128 (2017).

[25] S. Taie, H. Ozawa, T. Ichinose, T. Nishio, S. Nakajima, and Y. Takahashi, Coherent driving and freezing of bosonic matter wave in an optical Lieb lattice, Sci. Adv. **1**, e1500854 (2015).

[26] In the same way as the case of bosons [25], repulsively interacting fermionic isotopes of ytterbium (^{173}Yb) with two and six populated components at a temperature of around 20% of the Fermi temperature have been successfully loaded into a Lieb lattice, as confirmed by a band-mapping technique.

[27] C. Hofrichter, L. Riegger, F. Scazza, M. Höfer, D. R. Fernandes, I. Bloch, and S. Fölling, Direct Probing of the Mott Crossover in the SU(n) Fermi-Hubbard Model, Phys. Rev. X **6**, 021030 (2016).

[28] S. Taie, E. Ibarra-García-Padilla, N. Nishizawa, Y. Takasu, Y. Kuno, H.-T. Wei, R. T. Scalettar, K. R. A. Hazzard, and Y. Takahashi, Observation of antiferromagnetic correlations in an ultracold SU(n) Hubbard model, arXiv:2010.07730.

[29] S. Fuchs, E. Gull, L. Pollet, E. Burovski, E. Kozik, T. Pruschke, and M. Troyer, Thermodynamics of the 3D Hubbard Model on Approaching the Néel Transition, Phys. Rev. Lett. **106**, 030401 (2011).

[30] P. Törmä and K. Sengstock, *Quantum Gas Experiments – Exploring Many-Body States* (Imperial College Press, London, 2015).

[31] A. Mazurenko, C. S. Chiu, G. Ji, M. F. Parsons, M. Kanász-Nagy, R. Schmidt, F. Grusdt, E. Demler, D. Greif, and M. Greiner, A cold-atom Fermi–Hubbard antiferromagnet, Nature (London) **545**, 462 (2017).

[32] E. Cocchi, L. A. Miller, J. H. Drewes, C. F. Chan, D. Pertot, F. Brennecke, and M. Köhl, Measuring Entropy and Short-Range Correlations in the Two-Dimensional Hubbard Model, Phys. Rev. X **7**, 031025 (2017).

[33] S. Taie, T. Ichinose, H. Ozawa, and Y. Takahashi, Spatial adiabatic passage of massive quantum particles in an optical Lieb lattice, Nat. Commun. **11**, 257 (2020).

[34] S. Sugawa, K. Inaba, S. Taie, R. Yamazaki, M. Yamashita, and Y. Takahashi, Interaction and filling-induced quantum phases of dual Mott insulators of bosons and fermions, Nat. Phys. **7**, 642 (2011).

[35] G.-B. Jo, J. Guzman, C. K. Thomas, P. Hosur, A. Vishwanath, and D. M. Stamper-Kurn, Ultracold Atoms in a Tunable Optical Kagome Lattice, Phys. Rev. Lett. **108**, 045305 (2012).

[36] R. Drost, T. Ojanen, A. Harju, and P. Liljeroth, Topological states in engineered atomic lattices, Nat. Phys. **13**, 668 (2017).

[37] M. R. Slot, T. S. Gardenier, P. H. Jacobse, G. C. P. van Miert, S. N. Kempkes, S. J. M. Zevenhuizen, C. M. Smith, D. Vanmaekelbergh, and I. Swart, Experimental realization and characterization of an electronic Lieb lattice, Nat. Phys. **13**, 672 (2017).

[38] L. Yan and P. Liljeroth, Engineered electronic states in atomically precise artificial lattices and graphene nanoribbons, Adv. Phys. X **4**, 1651672 (2019).

[39] R. A. Vicencio, C. Cantillano, L. Morales-Inostroza, B. Real, C. Mejía-Cortés, S. Weimann, A. Szameit, and M. I. Molina, Observation of Localized States in Lieb Photonic Lattices, Phys. Rev. Lett. **114**, 245503 (2015).

[40] S. Mukherjee, A. Spracklen, D. Choudhury, N. Goldman, P. Öhberg, E. Andersson, and R. R. Thomson, Observation of a Localized Flat-Band State in a Photonic Lieb Lattice, Phys. Rev. Lett. **114**, 245504 (2015).

[41] F. Baboux, L. Ge, T. Jacqmin, M. Biondi, E. Galopin, A. Lemaître, L. Le Gratiet, I. Sagnes, S. Schmidt, H. E. Türeci, A. Amo, and J. Bloch, Bosonic Condensation and Disorder-Induced Localization in a Flat Band, Phys. Rev. Lett. **116**, 066402 (2016).

[42] C. E. Whittaker, E. Cancellieri, P. M. Walker, D. R. Gulevich, H. Schomerus, D. Vaitiekus, B. Royall, D. M. Whittaker, E. Clarke, I. V. Iorsh, I. A. Shelykh, M. S. Skolnick, and D. N. Krizhanovskii, Exciton Polaritons in a Two-Dimensional Lieb Lattice with Spin-Orbit Coupling, Phys. Rev. Lett. **120**, 097401 (2018).

[43] V. Goblot, B. Rauer, F. Vicentini, A. Le Boité, E. Galopin, A. Lemaître, L. Le Gratiet, A. Harouri, I. Sagnes, S. Ravets, C. Ciuti, A. Amo, and J. Bloch, Nonlinear Polariton Fluids in a Flatband Reveal Discrete Gap Solitons, Phys. Rev. Lett. **123**, 113901 (2019).

[44] T. Fukuhara, Y. Takasu, M. Kumakura, and Y. Takahashi, Degenerate Fermi Gases of Ytterbium, Phys. Rev. Lett. **98**, 030401 (2007).

[45] S. Taie, Y. Takasu, S. Sugawa, R. Yamazaki, T. Tsujimoto, R. Murakami, and Y. Takahashi, Realization of a SU(2) × SU(6) System of Fermions in a Cold Atomic Gas, Phys. Rev. Lett. **105**, 190401 (2010).

[46] G. Pagano, M. Mancini, G. Cappellini, P. Lombardi, F. Schäfer, H. Hu, X.-J. Liu, J. Catani, C. Sias, M. Inguscio, and L. Fallani, A one-dimensional liquid of fermions with tunable spin, Nat. Phys. **10**, 198 (2014).

[47] B. J. DeSalvo, M. Yan, P. G. Mickelson, Y. N. Martinez de Escobar, and T. C. Killian, Degenerate Fermi Gas of ^{87}Sr, Phys. Rev. Lett. **105**, 030402 (2010).

[48] S. Stellmer, R. Grimm, and F. Schreck, Production of quantum-degenerate strontium gases, Phys. Rev. A **87**, 013611 (2013).

[49] See Supplemental Material http://link.aps.org/supplemental/10.1103/PhysRevA.103.L031301 for details of the hopping matrix of the noninteracting Hamiltonian, calculation of the entropy and the double occupancy using DMFT, derivation of the scaling relation of Eq. (2), and more details on the trapping potential and the local density approximation used to obtain the result of Fig. 6, which includes Refs. [59–62].

[50] A. Georges, G. Kotliar, W. Krauth, and M. J. Rozenberg, Dynamical mean-field theory of strongly correlated fermion systems and the limit of infinite dimensions, Rev. Mod. Phys. **68**, 13 (1996).

[51] G. Kotliar and D. Vollhardt, Strongly correlated materials: Insights from dynamical mean-field theory, Phys. Today **57**(3), 53 (2004).

[52] U. Schneider, L. Hackermüller, S. Will, T. Best, I. Bloch, T. A. Costi, R. W. Helmes, D. Rasch, and A. Rosch, Metallic and insulating phases of repulsively interacting fermions in a 3D optical lattice, Science **322**, 1520 (2008).

[53] F. Werner, O. Parcollet, A. Georges, and S. R. Hassan, Interaction-Induced Adiabatic Cooling and Antiferromagnetism of Cold Fermions in Optical Lattices, Phys. Rev. Lett. **95**, 056401 (2005).

[54] S.-K. Yip, B.-L. Huang, and J.-S. Kao, Theory of SU(N) Fermi liquids, Phys. Rev. A **89**, 043610 (2014).

[55] R. C. Richardson, The Pomeranchuk effect, Rev. Mod. Phys. **69**, 683 (1997).

[56] S. Taie, R. Yamazaki, S. Sugawa, and Y. Takahashi, An SU(6) Mott Insulator of an atomic Fermi gas realized by large-spin Pomeranchuk cooling, Nat. Phys. **8**, 825 (2012).

[57] C. Lenihan, A. J. Kim, F. Šimkovic IV, and E. Kozik, Entropy in the non-Fermi-liquid regime of the doped 2d Hubbard model, arXiv:2001.09948.

[58] K.-E. Huhtinen and P. Törmä, Insulator-pseudogap crossover in the Lieb lattice, arXiv:2007.05118.

[59] F. F. Assaad and T. C. Lang, Diagrammatic determinantal guantum Monte Carlo methods: Projective schemes and applications to the Hubbard-Holstein model, Phys. Rev. B **76**, 035116 (2007).

[60] E. V. Gorelik, I. Titvinidze, W. Hofstetter, M. Snoek, and N. Blümer, Néel Transition of Lattice Fermions in a Harmonic Trap: A Real-Space Dynamic Mean-Field Study, Phys. Rev. Lett. **105**, 065301 (2010).

[61] E. Gull, Ph.D. thesis, ETH Zurich, 2008 (unpublished).

[62] E. Gull, A. J. Millis, A. I. Lichtenstein, A. N. Rubtsov, M. Troyer, and P. Werner, Continuous-time Monte Carlo methods for quantum impurity models, Rev. Mod. Phys. **83**, 349 (2011).